Electronic Supplementary Information for

Highly Efficient Electrocatalytic Hydrogen Evolution Promoted by O–Mo–C Interfaces of Ultrafine β-Mo_2C Nanostructures

Hui Yang,[ab] Xing Chen,[c] Guoxiang Hu,[d] Wan-Ting Chen,[e] Siobhan J. Bradley,[f] Weijie Zhang,[b] Gaurav Verma,[b] Thomas Nann,[f] De-en Jiang,[g] Paul E. Kruger,[h] Xiangke Wang,[a] He Tian,*[c] Geoffrey I. N. Waterhouse,[e] Shane G. Telfer,[i] and Shengqian Ma*[b]*

[a]College of Environmental Science and Engineering, North China Electric Power University, Beijing, 102206, P. R. China.
E-mail: xkwang@ncepu.edu.cn

[b]Department of Chemistry, University of South Florida 4202 E. Fowler Avenue, Tampa, Florida 33620, United States.
E-mail: sqma@usf.edu

[c]Center of Electron Microscopy, Zhejiang University, Hangzhou 310027, P.R. China.
E-mail: hetian@zju.edu.cn

[d]Center for Nanophase Materials Sciences, Oak Ridge National Laboratory, Oak Ridge, Tennessee 37831, United States.

[e]MacDiarmid Institute for Advanced Materials and Nanotechnology, School of Chemical Sciences, The University of Auckland, Auckland 1142, New Zealand.

[f]MacDiarmid Institute for Advanced Materials and Nanotechnology, School of Chemical and Physical Sciences, Victoria University of Wellington, Wellington 6140, New Zealand.

[g]Department of Chemistry, University of California, Riverside, California 92521, United States.

[h]MacDiarmid Institute for Advanced Materials and Nanotechnology, School of Physical and Chemical Sciences, University of Canterbury, Christchurch 8140, New Zealand, New Zealand.

[i]MacDiarmid Institute for Advanced Materials and Nanotechnology, Institute of Fundamental Sciences, Massey University, Palmerston North 4442, New Zealand.

Chemicals

All reagents and solvents were sourced from commercial suppliers and used without further purification, unless otherwise noted.

Instrumentation

Powder X-ray diffraction (PXRD) data were collected on a Bruker AXS X-ray diffractometer equipped with a Cu Kα source. BET surface areas were determined from N_2 adsorption/desorption isotherms obtained at 77 K using a Micromeritics ASAP2020. Before analysis, samples were pre-treated *in vacuo* at 100 °C for 1000 min. Scanning electron microscopy (SEM) images and energy dispersive spectra (EDS) were recorded on a Hitachi 800 Scanning Electron Microscope with an EDS module. Transmission electron microscopy (TEM) images were recorded on FEI Tecnai G^2 BioTwin transmission electron microscope operating at an accelerating voltage of 100 kV. Scanning transmission electron microscopy (STEM) and EDS mapping analyses were carried out on a JEOL JEM-2100F transmission electron microscope operating at an accelerating voltage of 200 kV. High-angle annular dark-field (HAADF) images were obtained using a Titan G2 80-200 ChemiSTEM scanning transmission electron microscope operating at 200 kV and equipped with a probe spherical aberration corrector. Inductively coupled plasma atomic emission spectroscopy (ICP-AES) analyses were performed on a Jobin Yvon Horiba-Ultima 2 spectrometer system. Elemental Analyses (EA) were performed on a Vario MICRO analysis system. Raman spectra were measured from powder samples using a Cobalt Samba single-mode 532 nm diode laser interfaced with a DXR SmartRama spectrometer. X-ray photoelectron spectroscopy (XPS) analyses were performed using a Kratos Axis DLD spectrometer, equipped with a monochromatic Al Kα X-ray source. Fourier transform infrared spectra (FTIR) were recorded on a ThermoElectron Nicolet high-resolution FT-MIR/FT-FarIR. X-ray absorption structure spectra were collected in transmission mode on beamline 10BM-B of the Advanced Photon Source (APS). The HER tests were performed with PINE (AFMSRCE Electrode Rotator WaveDriver 20 Bipotentiostat/Galvanostat System, USA) and VersaSTAT 4 Potentiostat Galvanostat electrochemical analysers.

Experimental section

Synthesis of NPCC

A nitrogen-doped porous carbon capsule (NPCC) was prepared by direct pyrolysis of the ZIF-8@K-TA composite. The pyrolysis conditions were identical to those described for the synthesis of β-Mo_2C@NPCC.

Electrochemical Tests

All electrochemical measurements were conducted in a standard three−electrode system with a graphite rod counter

electrode and Ag/AgCl (3.5 M KCl) reference electrode. The working electrode comprised a glassy carbon (GC) rotating disk electrode (RDE, 5.0 mm in diameter, 0.196 cm^2, PINE, USA) functionalized with the as–synthesized electrocatalysts. To prepare the working electrode, 5 mg of β-Mo_2C@NPCC or 10 mg of Pt/C (a commercially available 20 wt% Pt/C catalyst) were dispersed in 1.1 mL of ethanol and 100 µL of deionized water (containing 50 µL of 5.0 wt% Nafion solution) under ultrasonic agitation to form an electrocatalyst ink. The ink was then dropped on the surface of the pre-cleaned rotating disk working electrode and dried at room temperature. The catalyst loading was determined to be 0.1 mg cm^{-2} (based on catalyst mass). For all electrochemical tests, the working electrode rotation rate was 1600 rpm. Linear sweep voltammetry (LSV) curves were recorded in nitrogen-saturated H_2SO_4 (0.5 M) or KOH (1 M) electrolytes at scan rates of 5 mV s^{-1}. Long-term stability tests for catalysts were conducted for 3000 cycles by measuring polarization curves at 50 mV s^{-1} with LSV technique. Electrochemical impedance spectroscopy (ESI) measurements were carried out from 10^5 to 10^{-2} Hz and an amplitude of 10 mV (versus RHE). The double-layer capacitances (C_{dl}) were obtained from cyclic voltammograms (CV) curves collected at scan rates ranging from 20 to 200 mV s^{-1} in the potential region from 0.1 to 0.3 V (versus RHE).

Table S1 Summarized elemental composition data and N_2 physisorption data for the as-synthesized β-Mo_2C@NPCC and NPCC electrocatalysts.

material	precursor	Mo (wt %)	N (wt %)	BET[b]	Pore vol.[c]
β-Mo_2C@NPCC	ZIF-8@Mo-TA	4.07	3.0	670	0.66
NPCC	ZIF-8@K-TA	n/a[a]	3.8	1164	1.02

[a]n/a = not applicable; [b]BET surface area in m^2/g determined by N_2 adsorption at 77 K. [c]Total pore volume in cm^3/g determined by N_2 adsorption at 77 K.

Materials Characterization

Powder X-ray Diffraction (PXRD)

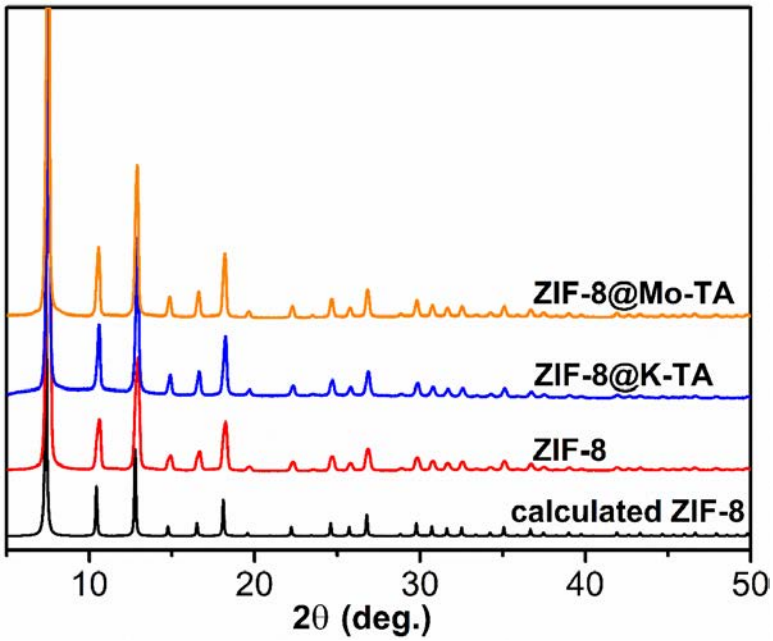

Fig. S1 PXRD patterns of the as-synthesized materials. The calculated pattern for ZIF-8 is also shown.

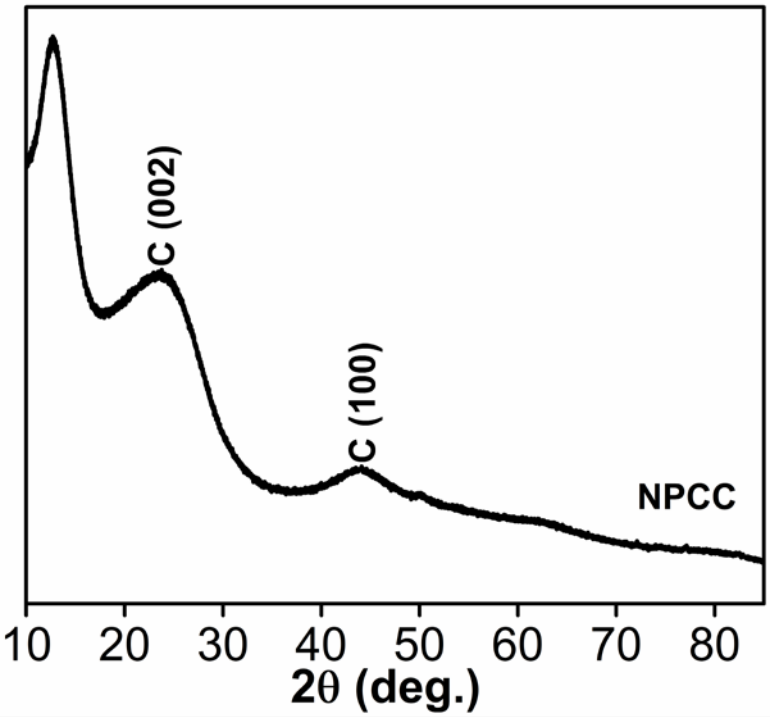

Fig. S2 PXRD pattern of as-synthesized NPCC.

Scanning Electron Microscopy (SEM) and Transmission Electron Microscopy (TEM)

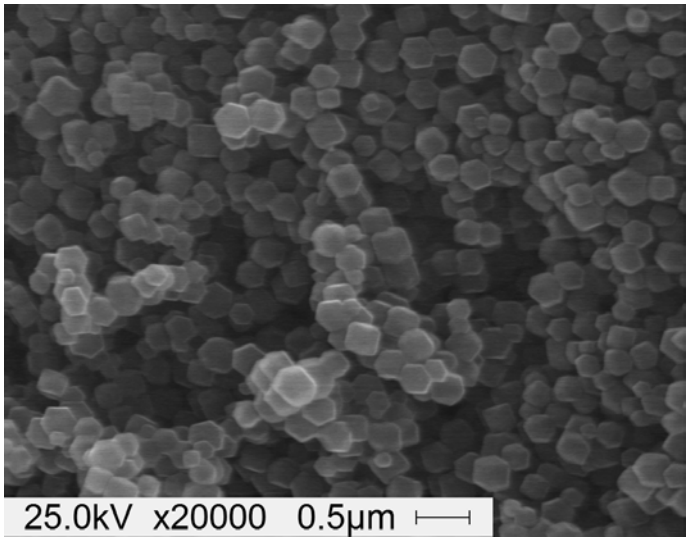

Fig. S3 SEM image of ZIF-8 nanocrystals.

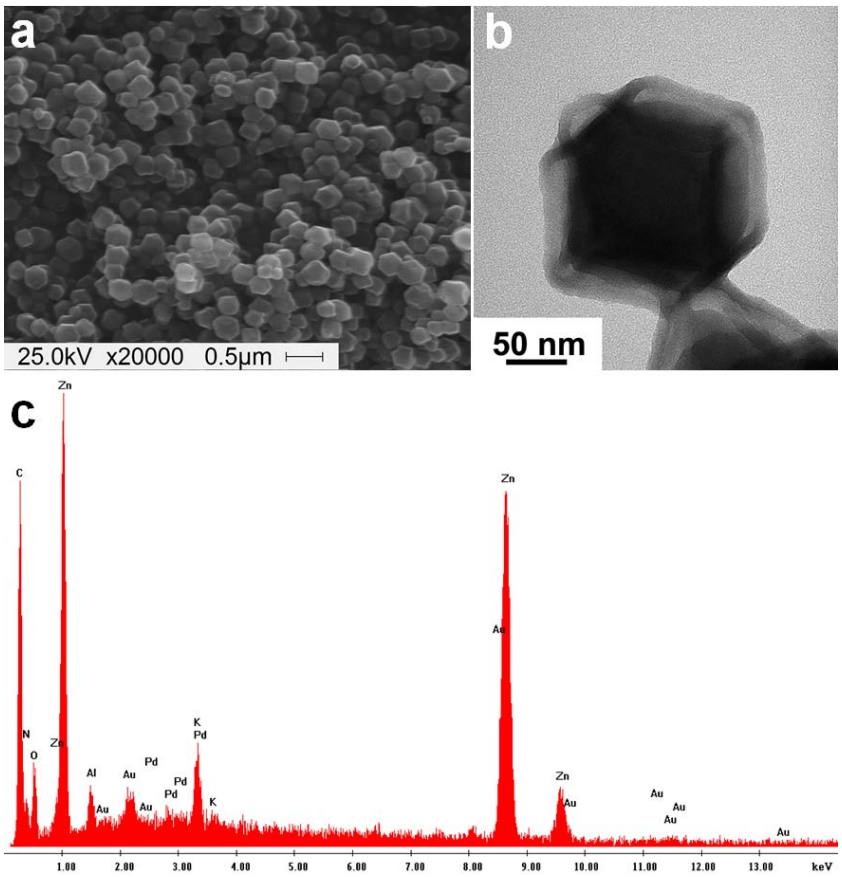

Fig. S4 SEM image (a), TEM image (b) and EDS spectrum (c) of ZIF-8@K-TA.

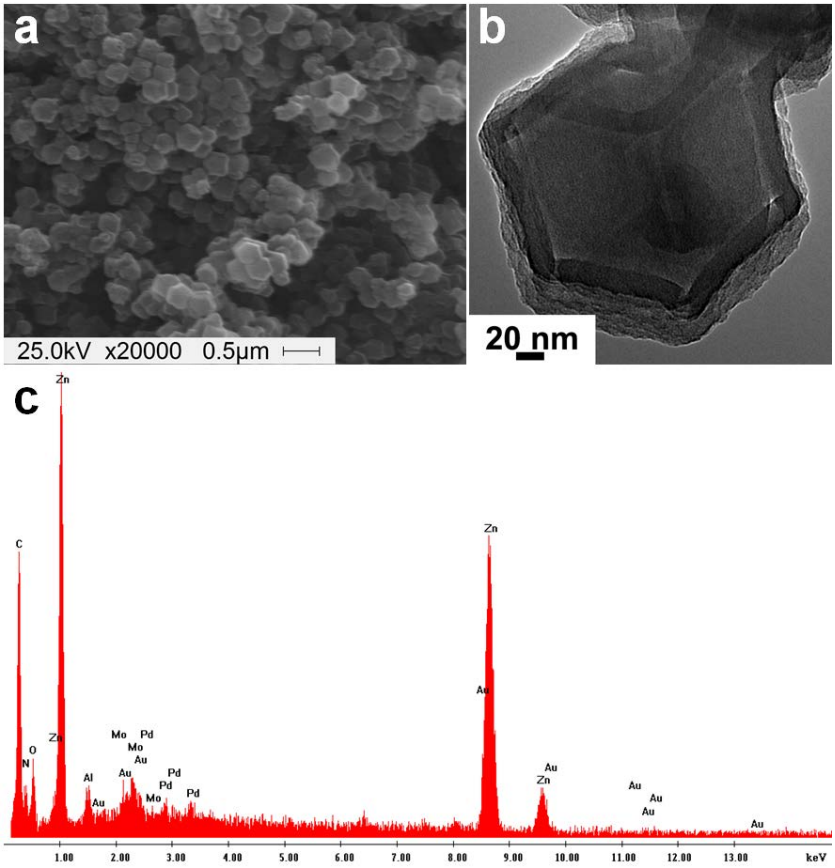

Fig. S5 SEM image (a), TEM image (b) and EDS spectrum (c) of ZIF-8@Mo-TA.

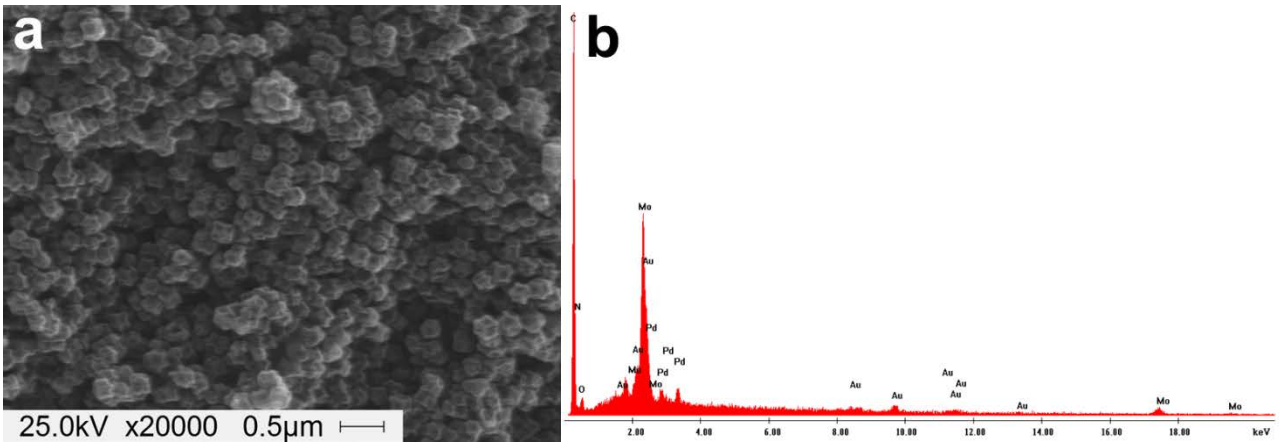

Fig. S6 SEM image (a) and EDS spectrum (b) of β-Mo_2C@NPCC.

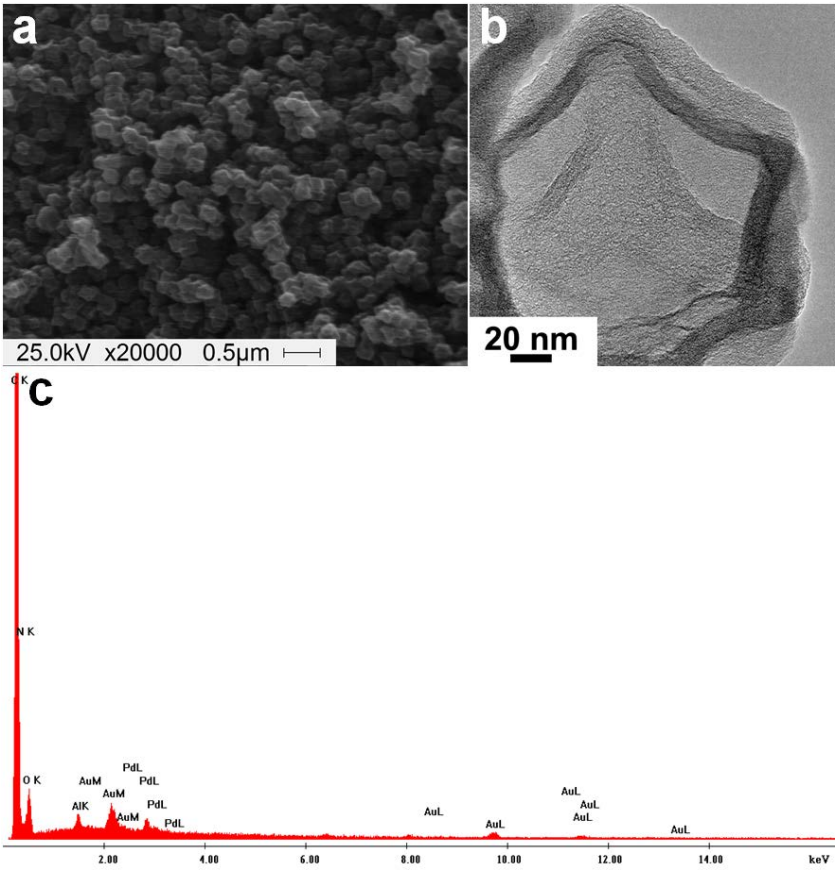

Fig. S7 SEM image (a), TEM image (b) and EDS spectrum (c) of NPCC.

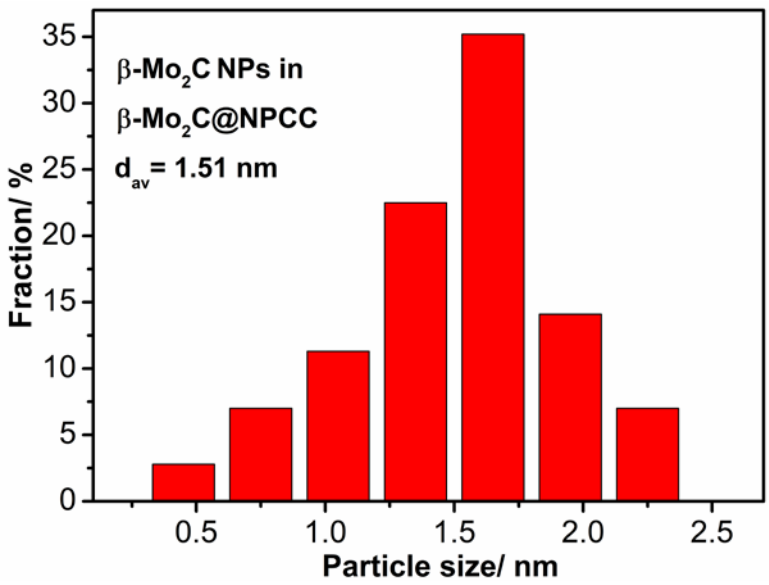

Fig. S8 Histogram of nanoparticle sizes in β-Mo_2C@NPCC.

Fourier Transform Infrared (FT-IR) Spectroscopy

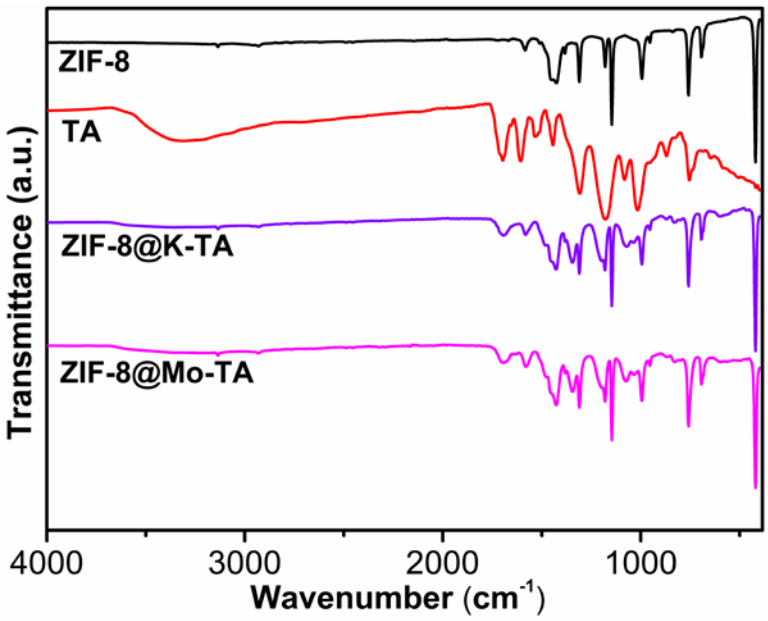

Fig. S9 FTIR spectra of each material.

X-ray Photoelectron Spectroscopy (XPS)

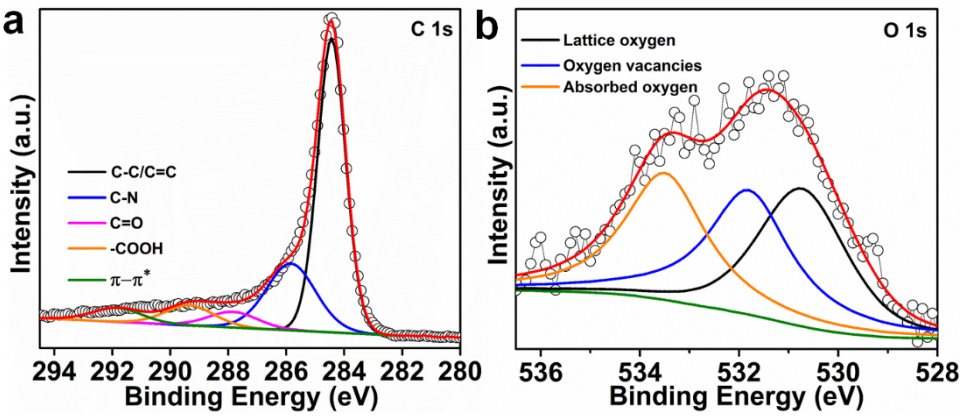

Fig. S10 C 1s (a) and O 1s (b) XPS spectra of β-Mo_2C@NPCC.

Table S2 Summarised XPS results of β-Mo_2C@NPCC.

Elements	Peak position (eV)	Relative area (%)
	Mo 3d region	
Mo^{2+} $3d_{5/2}$ from Mo_2C	228.3	26.24
Mo^{2+} $3d_{3/2}$ from Mo_2C	231.4	17.49
Mo^{3+} $3d_{5/2}$ from Mo_2N	229.1	13.18
Mo^{3+} $3d_{3/2}$ from Mo_2N	232.8	8.79
Mo^{6+} $3d_{5/2}$ from Mo-O	232.2	20.58
Mo^{6+} $3d_{3/2}$ from Mo-O	235.9	13.72
	C 1s region	
C-C/C=C	284.4	58.97
C-N	285.9	23.54
C=O	287.8	5.53
$-CO_2H$	289.4	7.04
π-π*	292.0	4.92
	N 1s region	
Mo $3p_{3/2}$	394.3	33.72
N-Mo	396.1	14.30
Pyridinic N	398.1	26.91
Pyrrolic N	400.1	3.25
Graphite N	401.0	18.63
Pydridinic oxide, N-O	403.6	3.19

X-ray Absorption Spectroscopy (XAS) Measurements

Mo K-edge X-ray absorption spectra were collected in transmission mode on beamline 10BM-B of the Advanced Photon Source (APS). A Hitachi Vortex-ME4 four-element silicon drift fluorescence detector was used. For all samples, data sets were collected until an adequate signal-to-noise was obtained, in all instances requiring between 3 and 10 scans. The X-ray white light beam was monochromatized by a Si (111) monochromator and detuned by 50% to reduce the contribution of higher-order harmonics. All data were collected at ambient temperature.

EXAFS Analysis and Results

The Mo K-edge absorption spectra were processed with the Athena and Artemis programs of the IFEFFIT package.[1] Reference foil data were aligned to the first zero-crossing of the second derivative of normalized $\mu(E)$ data, which was calibrated to the literature E_0 value for the molybdenum K-edge. Spectra were averaged in $\mu(E)$ prior to normalization. Background removal was achieved by spline fitting.

Mo K-edge extended X-ray absorption fine structure (EXAFS) data were extracted from the absorption spectra above the threshold energy (E_0). FEFF 9 was used to calculate theoretical phases and amplitudes from structure models consisting of crystal structures or the Cartesian coordinates of geometrically optimized computational models. All data were initially fitted with simultaneous k-weighting of 1, 2, and 3, then finalized with k^3-weighting in R-space. Fit windows in k-space were determined based on the lowest quality data collected, and for all data sets were from 0 - 12 $Å^{-1}$. Fit windows in R-space were determined on a case-by-case basis, based on the features apparent in the spectrum. In all fits, the amplitude reduction factor (S_0^2) and the energy shift of the photoelectron (ΔE_0) were global parameters. Independent structural parameters determined by the fits included the change in the scattering half path length (R) and the relative mean square displacement of the scattering element (σ^2). For each fit, the number of variables was not permitted to exceed 2/3 the number of independent points, in keeping with the Nyquist criterion.

Mo L-edge XANES spectra were collected in the partial electron yield (PEY) mode on the Soft X-ray beamline at the Australian Synchrotron. The PEY data were normalized against a current measured simultaneously on a gold mesh in the beamline to eliminate potential spectral artefacts caused by fluctuations in the beam intensity whilst scanning. Samples were sprinkled on carbon adhesive tape for the analyses.

Table S3 Summarized Mo K-edge EXAFS curve fitting parameters for β-Mo_2C@NPCC.

material	path	[a]*CN*	[b]*R* (Å)	[c]σ^2 (Å)	[d]*ΔE*	[e]*R-factor (%)*
β-Mo_2C@NPCC	Mo-O	2.0 (0.02)	1.670 (0.020)	0.003 (0.0003)	-1.08 (0.74)	0.012
	Mo-O	2.0 (0.87)	2.332 (0.009)	0.001 (0.0005)	-1.08 (0.74)	0.012
	Mo-C	1.0 (0.50)	2.135 (0.017)	0.005 (0.0008)	-1.08 (0.74)	0.012
	Mo-Mo	2.0 (0.18)	3.019 (0.006)	0.008 (0.0002)	-1.08 (0.74)	0.012

[a]*CN*, coordination number; [b]*R*, distance between absorber and backscatter atoms; [c]σ^2, Debye–Waller factor to account for both thermal and structural disorders; [d]ΔE_0, inner potential correction, [e]*R* factor (%), indicates the goodness of the fit.

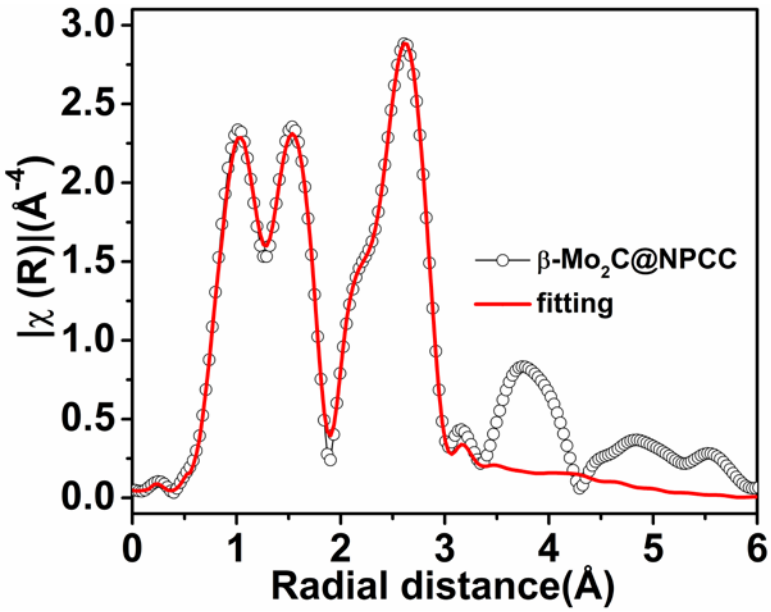

Fig. S11 Mo K-edge *R* space EXAFS data and curve fit for β-Mo_2C@NPCC.

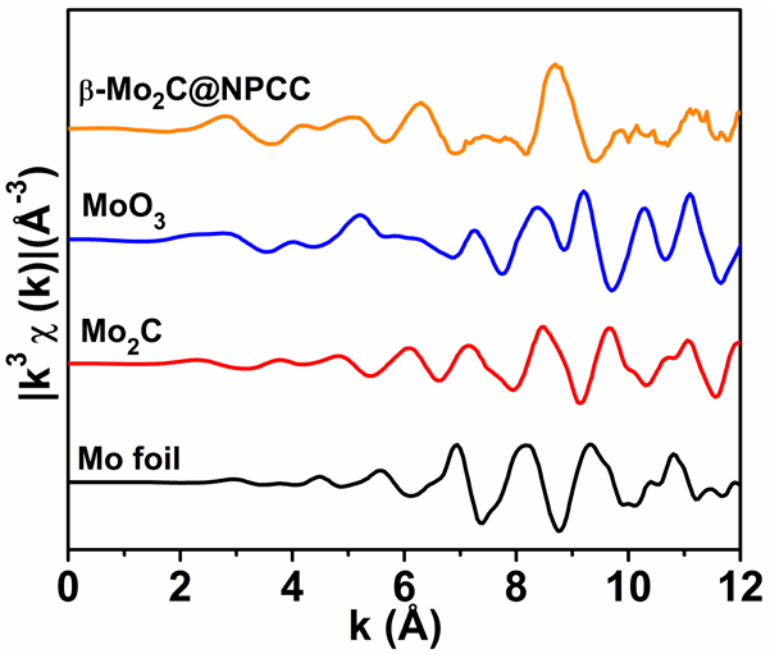

Fig. S12 Mo K-edge *k* space EXAFS data of β-Mo_2C@NPCC together with Mo foil, Mo_2C and MoO_3.

Raman Spectroscopy

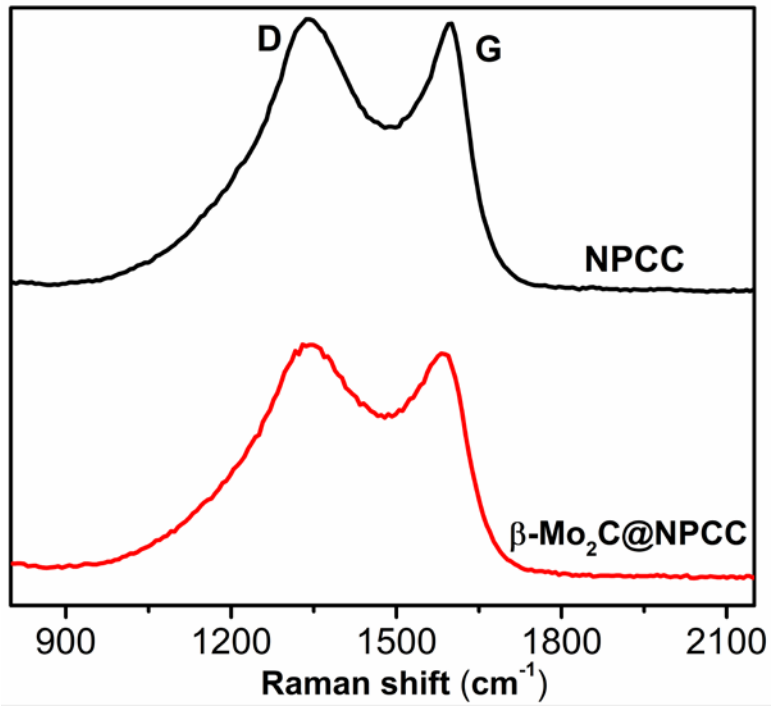

Fig. S13 Raman spectra for NPCC and β-Mo_2C@NPCC.

Nitrogen Physisorption Measurements and Pore Size Analyses

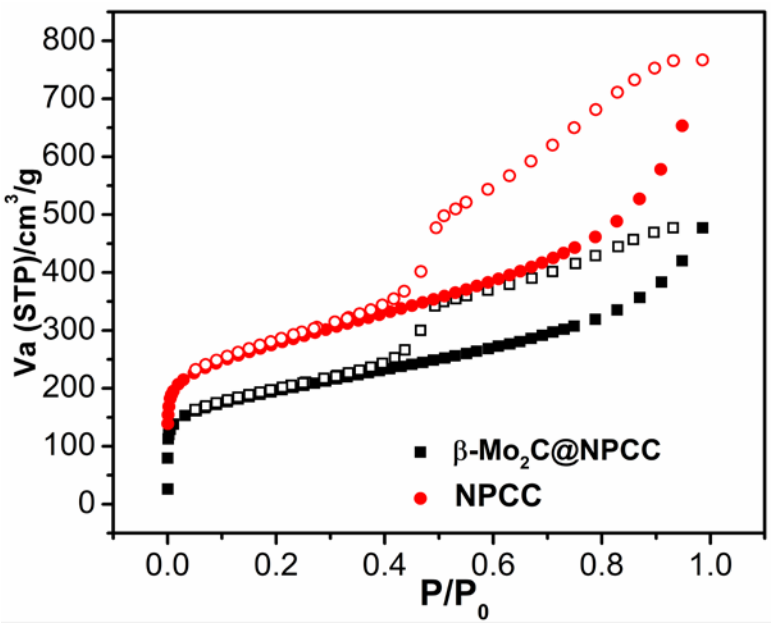

Fig. S14 N_2 adsorption (filled symbols) and desorption (open symbols) isotherms measured at 77 K for β-Mo_2C@NPCC and NPCC.

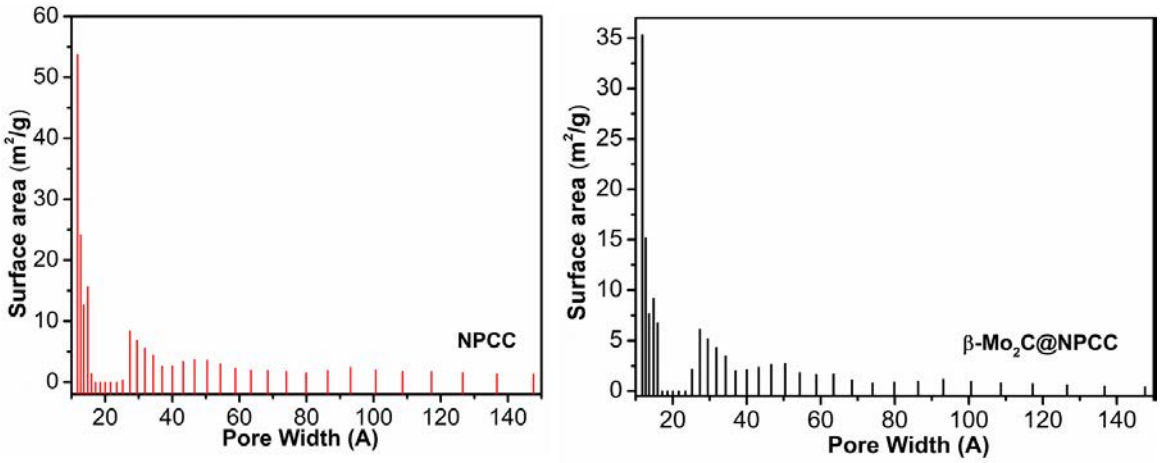

Fig. S15 Pore size distribution plots calculated using a DFT method from N_2 isotherms measured at 77 K for NPCC and β-Mo_2C@NPCC.

Hydrogen Evolution Reaction (HER)

Turnover Frequency (TOF) Calculations:

The TOF, i.e. the number of H_2 molecules generated per second from each Mo active site, was calculated according to the following equation:

$$TOF = \frac{total\ hydrogen\ turnovers\ per\ geometric\ area}{active\ sites\ per\ geometric\ area}$$

The total hydrogen turnover can be calculated from the current density (*j*) extracted from the LSV polarization curve according to:

$$total\ H_2\ turnover = \left(j\frac{mA}{cm^2}\right)\left(\frac{1C/s}{1000\ mA}\right)\left(\frac{1\ mol\ e}{96485.3\ C}\right)\left(\frac{1\ mol}{2\ mol\ e}\right)\left(\frac{6.022 * 10^{23} molecules\ H_2}{2\ mol\ e}\right)$$

therefore

$$total\ H_2\ turnover\ per\ unit\ j = 3.12 * 10^{15}\frac{H_2/s}{cm^2}per\frac{mA}{cm^2}$$

The number of Mo active sites in the β-Mo_2C@NPCC catalyst was calculated from the mass loading on the glassy carbon electrode. β-Mo_2C@NPCC contains 4.07 wt% molybdenum, and assuming each Mo center accounts for one accessible active site:

$$active\ sites = \left(\frac{catalyst\ loading\ per\ geometric\ area * Mo\%}{Mo\ M_W}\right)\left(\frac{6.022 * 10^{23} Mo\ atoms}{1\ mol\ Mo}\right)$$

$$= \frac{1 * 10^{-4} g/cm^2 * 4.07 wt\%}{95.94\ g/mol}\left(\frac{6.022 * 10^{23} Mo\ atoms}{1\ mol\ Mo}\right)$$

$$= 2.55 * 10^{16}\ atomic\ Mo\ sites\ per\ cm^2$$

Finally, the TOF in units of s^{-1} can be calculated from the current density (*j*) at any overpotential of interest according to:

$$TOF = \frac{total\ H_2\ turnover}{atomic\ sites\ per\ cm^2} = \left(\frac{3.12 * 10^{15} * j}{2.55 * 10^{16}}\right)$$

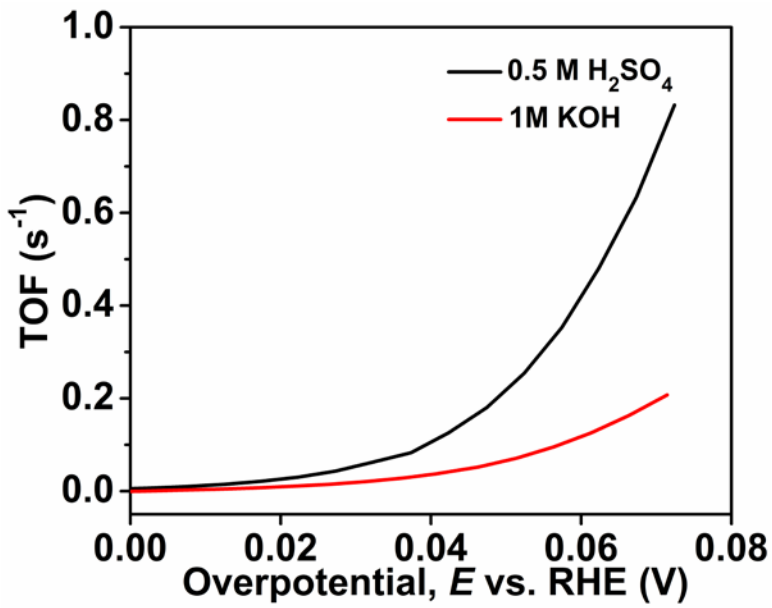

Fig. S16 TOF plots for β-Mo_2C@NPCC.

Table S4 Summary of the HER activities of the various catalysts tested in this work.

catalyst	electrolyte	onset η (mV versus RHE)	HER η@10 mA[b]	HER Tafel slope[c]
β-Mo_2C@NPCC	0.5 M H_2SO_4	36	80	40
NPCC	0.5 M H_2SO_4	90	216	n/d
commercial Pt/C	0.5 M H_2SO_4	0	43	31
β-Mo_2C@NPCC	1 M KOH	51	132	49
NPCC	1 M KOH	120	296	n/d
commercial Pt/C	1 M KOH	0	53	35

[a]n/a = not determined [b]HER η@10 mA cm^{-2} = the overpotential in mV for the hydrogen evolution reaction at a current density of 10 mA cm^{-2}. [c]In mV dec^{-1}.

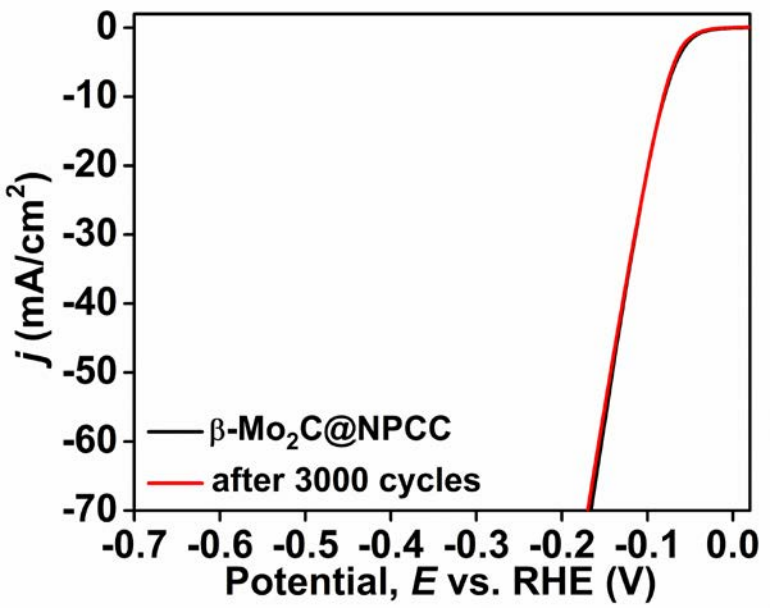

Fig. S17 Polarization curves for β-Mo_2C@NPCC before and after 3000 cycles testing in 0.5 M H_2SO_4 solution. The overpotential was used without *iR* correction.

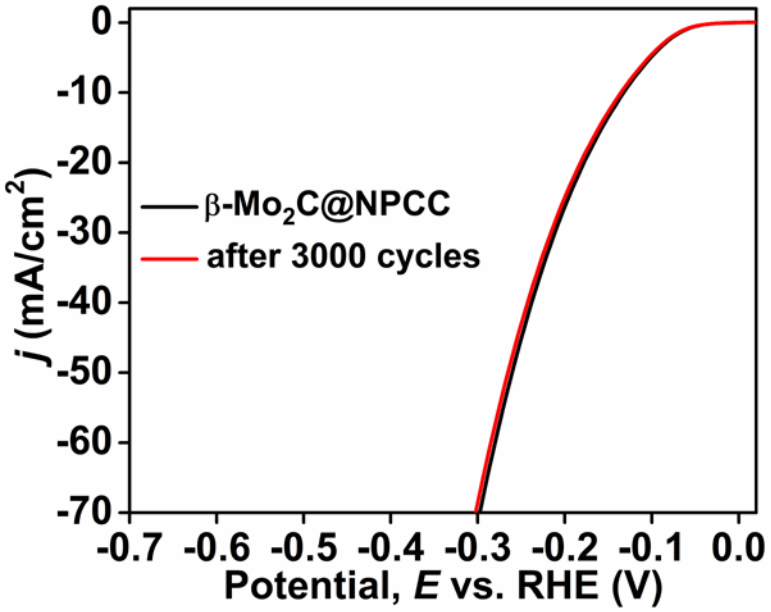

Fig. S18 Polarization curves for β-Mo_2C@NPCC before and after 3000 cycles testing in 1 M KOH solution. The overpotential was used without *iR* correction.

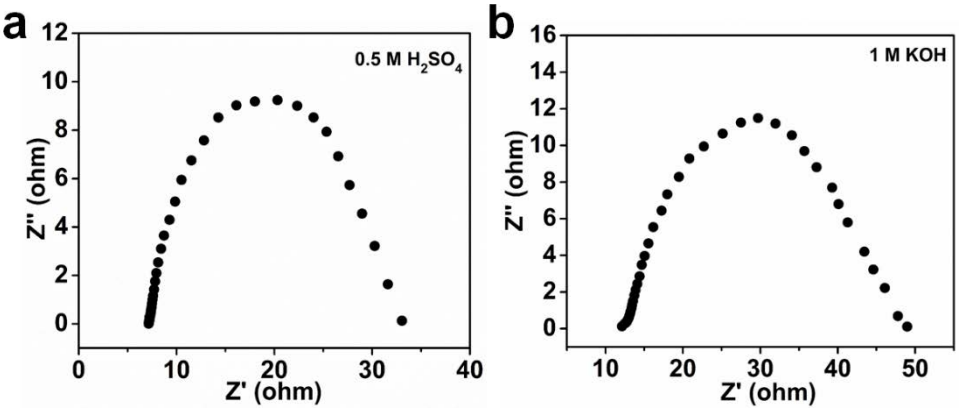

Fig. S19 EIS for β-Mo_2C@NPCC at an overpotential of 150 mV in 0.5 M H_2SO_4 (a) and 1M KOH (b). The overpotential was used without *iR* correction.

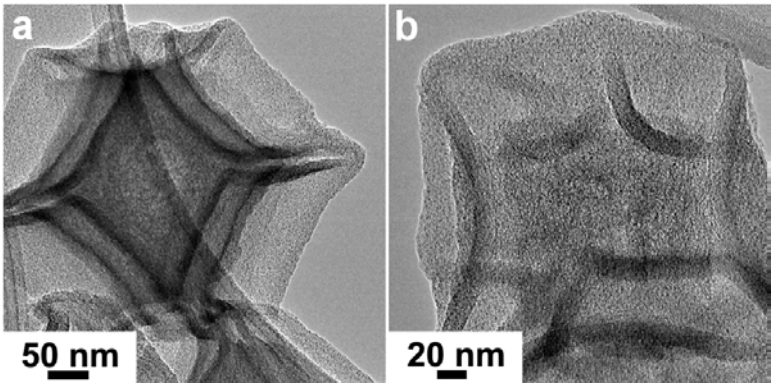

Fig. S20 TEM images of β-Mo_2C@NPCC after 3000 cycles of electrocatalytic hydrogen evolution in 0.5 M H_2SO_4 (a) and 1M KOH (b).

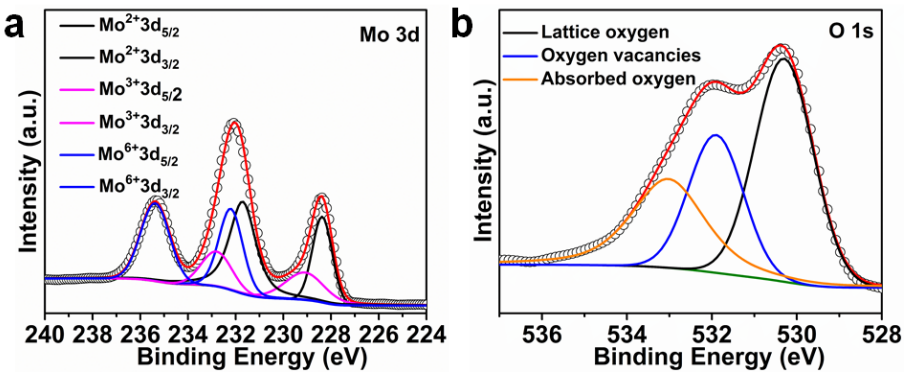

Fig. S21 Mo 3d (a) and O 1s (b) XPS spectra of β-Mo_2C@NPCC after cycles of electrocatalytic hydrogen evolution in 0.5 M H_2SO_4.

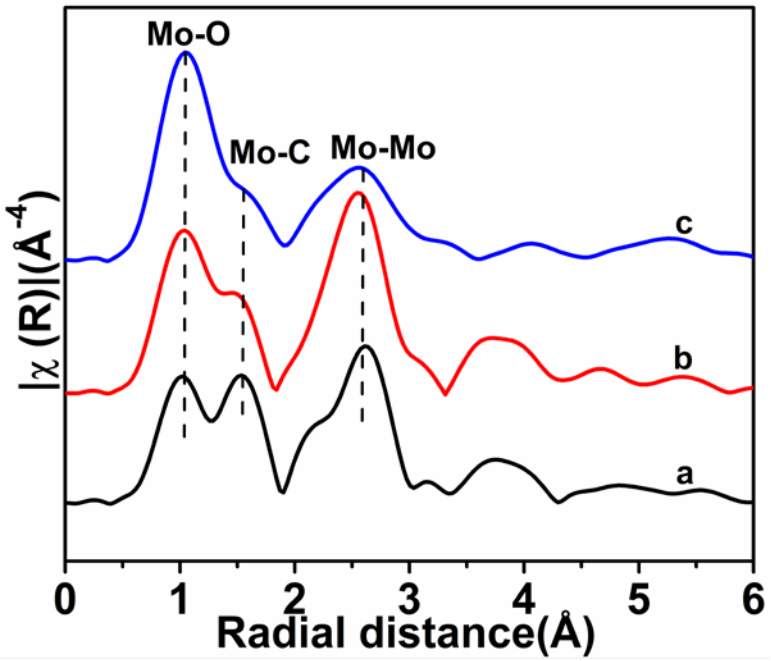

Fig. S22 Mo K-edge (*R* space) EXAFS spectra of β-Mo_2C@NPCC (a), after refluxing in 2 M H_2SO_4 for 24 h (b), and after refluxing in 4 M KOH for 24 h(c).

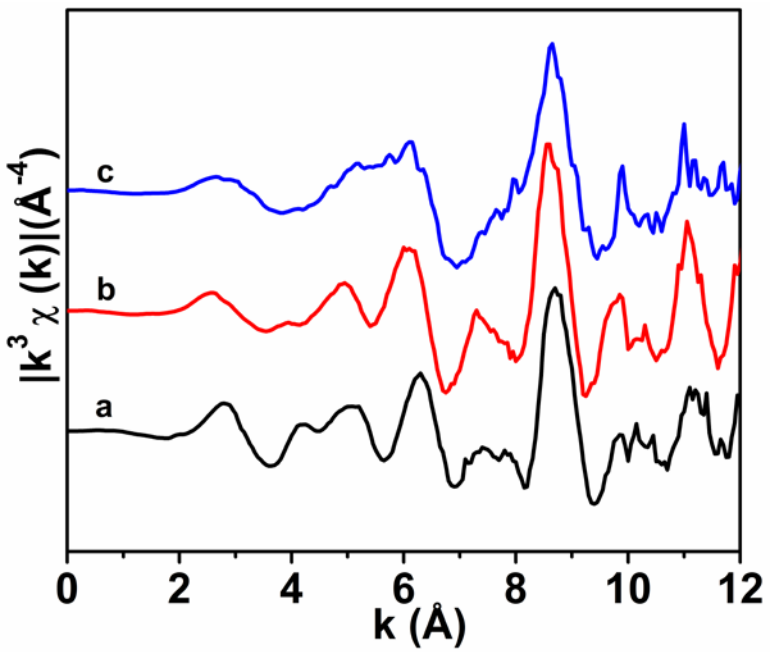

Fig. S23. Mo K-edge (*k* space) EXAFS spectra of β-Mo_2C@NPCC (a), after refluxing in 2 M H_2SO_4 for 24 h (b), and after refluxing in 4 M KOH for 24 h(c).

Density functional theory (DFT) calculations

For further insights into the excellent electrocatalytic performance of the β-Mo_2C@NPCC catalyst, DFT calculations were used to calculate the H adsorption free energies (ΔG_H) on theoretical structural models of the catalyst. Spin-polarized DFT calculations were performed using the Vienna *ab initio* simulation package (VASP).[2] Electron exchange-correlation was represented by the functional of Perdew, Burke and Ernzerhof (PBE) based on a generalized gradient approximation (GGA).[3] The ion-electron interaction was described with the projector augmented wave (PAW) method.[4] A cutoff energy of 400 eV was used for the plane-wave basis set. The Brillouin zone was sampled by (3×3×1) Monkhorst-Pack k-point mesh. The convergence threshold for structural optimization was set to be 0.025 eV/Å in force. The calculated lattice parameters of β-Mo_2C (a = 5.23 Å, b = 6.06 Å, and c = 4.73 Å) were in good agreement with the experimental values (a = 5.20 Å, b = 6.02 Å, and c = 4.73 Å).[5] The (001) facet with Mo-termination was adopted to act as the active surface for the β-Mo_2C nanoparticle (Ref 53, 60). The β-Mo_2C (001) surface is among the most stable and exposed surfaces of β-Mo_2C (Jiao, et al. *J. Phys. Chem. C,* 2011, 115, 45, 22360-22368). In addition, it is the most frequently used surface of β-Mo_2C for catalysis studies, because it is most densely packed, has unified active centers, and flat (Sholl, et al. *J. Phys. Chem. C,* 2011, 115, 14, 6870-6876). The β-Mo_2C (001)z was modelled by a slab with three layers of Mo-C atoms in a (4 × 4) lateral cell. During the structural optimizations, the atoms in the bottom two layers were fixed while the other atoms including the adsorbed H were fully relaxed. A vacuum space with a length of 15 Å was employed along the z-direction.

The Gibbs free energy of hydrogen adsorption ΔG_H was obtained by

$$\Delta G_H = E(catalyst + H) - E[catalyst] - \frac{1}{2}E(H_2) + \Delta E_{ZPE} - T\Delta S_H$$

where $E(catalyst + H)$ represents the total energy of the catalyst with one adsorbed H, and $E[catalyst]$ represents the total energy of the catalyst without H. $E(H_2)$ is the total energy of one gas phase H_2 molecule. ΔE_{ZPE} is the difference in zero-point energy between the adsorbed H and H in the gas phase H_2 molecule, and ΔS_H is the entropy difference between the adsorbed H and $\frac{1}{2}H_2$ in the gas phase at the standard condition. The zero-point energy was calculated by summing vibrational frequencies ω_v over all normal modes v: $E_{ZPE} = \frac{1}{2}\sum \hbar\omega_v$. The entropy of the free H_2 molecule at 298.15 K and 1 atm was taken from the NIST database[6], while for the adsorbed H, the vibrational entropy was considered and calculated by the methods described by Cramer.[7] We have tested all the possible H adsorption sites on β-Mo2C (001), and the most favorable adsorption site was found to be the Mo hollow site (as shown in Fig. S24a). The computed ΔG_H for the Mo hollow site was reported in Figure 5b, and it is also in good agreement with previous studies.

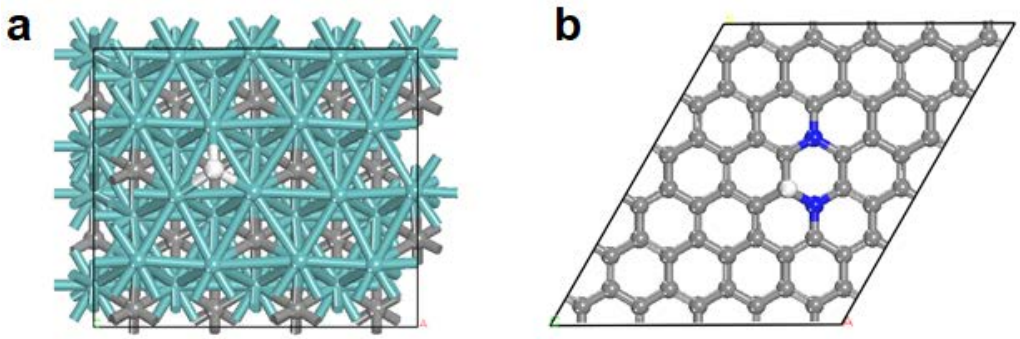

Fig. S24 The theoretical models used in DFT calculations and the adopted adsorption sites of H on the surface of these models: (a) β-Mo_2C and (b) NPCC. Mo (dark cyan), N (blue), C (grey), H (white).

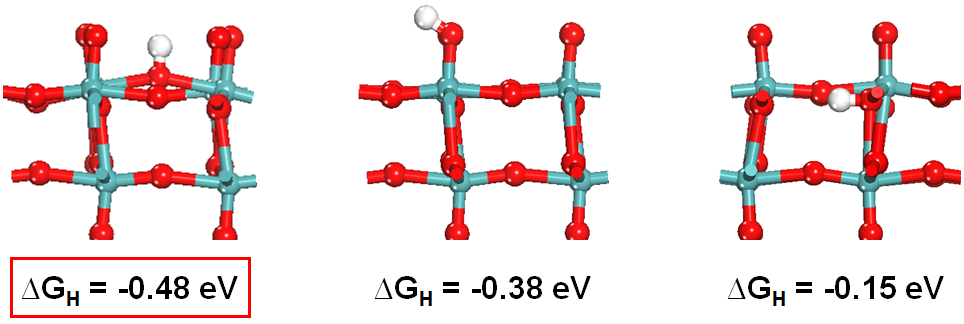

Fig. S25 The theoretical models used in DFT calculations and the adopted adsorption sites of H on the surface of MoO_3. Mo (dark cyan), O (red), H (white).

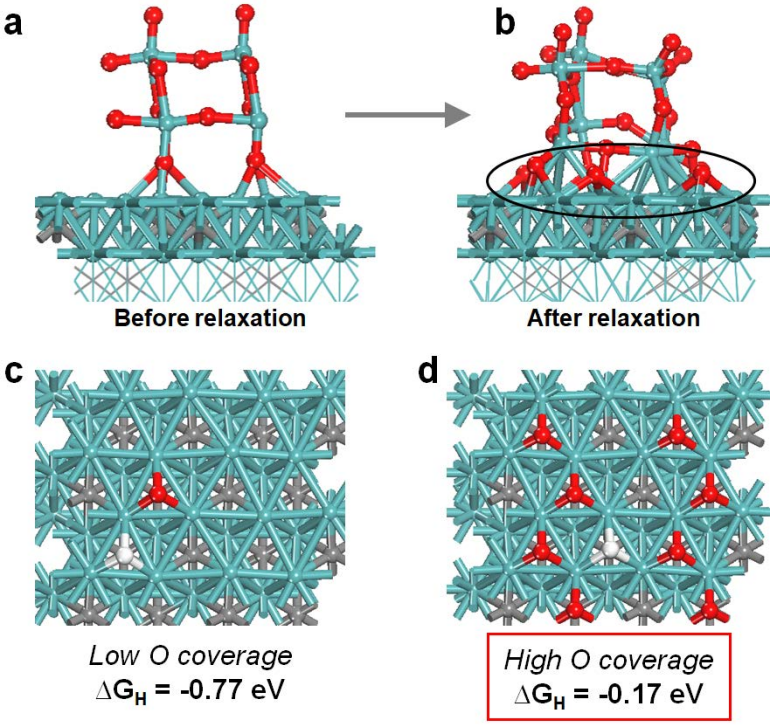

Fig. S26 The theoretical models used in DFT calculations and the adopted adsorption sites of H on the surface of O–Mo–C

interface. Mo (dark cyan), C (grey), O (red), H (white).

Table S5 Summary of the slab models, adsorption sites, and corresponding ΔG_H values studied in this work.

catalyst	slab model	adsorption site	ΔG_H (eV)
β-Mo_2C	(001) facet with Mo-termination	Mo hollow site	-0.85
MoO_3	(010) facet	two coordinated O site	-0.48
O-Mo-C interface	β-Mo_2C(001) with high O coverage	Mo hollow site	-0.17
NPCC	nitrogen-doped graphene	C top site nearest to N	0.69

Table S6 Summary of the electrocatalytic HER performance of different MoC_x materials

catalyst	overpotential (mV) η at j = 10 mA cm^{-2} (mV)	electrolyte	reference
β-Mo_2C@NPCC	80	0.5 M H_2SO_4	This work
β-Mo_2C@NPCC	132	1 M KOH	This work
Mo_2C@NC[8]	124	0.5 M H_2SO_4	*Angew. Chem. Int. Ed.* **2015**, *54,* 10752
Mo_2C@NC[8]	60	1 M KOH	*Angew. Chem. Int. Ed.* **2015**, *54,* 10752
mesoporous MoC_x nanooctahedron[9]	142	0.5 M H_2SO_4	*Nat. Commun.* **2015**, *6*, 6512
mesoporous MoC_x nanooctahedron[9]	151	1 M KOH	*Nat. Commun.* **2015**, *6*, 6512
MoCN[10]	145	H_2SO_4 (pH 1)	*J. Am. Chem. Soc.* **2015**, *137,* 110
MoCN-3D[11]	89	0.5 M H_2SO_4	*NPG Asia Mater.* **2016**, *8, e*293
MoCN-3D[11]	122	1 M KOH	*NPG Asia Mater.* **2016**, *8, e*293
β-Mo_2C nanotubes[12]	157	0.5 M H_2SO_4	*Angew. Chem. Int. Ed.* **2015**, *54,* 15395
β-Mo_2C[13]	189	0.1 M $HClO_4$	*Angew. Chem. Int. Ed.* **2014**, *53,* 6407
Mo_2C/CNT-graphene[14]	136	0.5 M H_2SO_4	*ACS Nano.* **2014**, *8,* 5164
Mo_2C nanowire[15]	131	0.5 M H_2SO_4	*Energy Environ. Sci.,* **2014**, *7,* 387
Mo_2C/CNT[16]	150	0.1 M $HClO_4$	*Energy Environ. Sci.,* **2013**, *6,* 943
3D Mo_xC/Ni network[17]	150	0.5 M H_2SO_4	*ChemCatChem,* **2014**, *6,* 2059.
Mo_2C/GCSs[18]	210	0.5 M H_2SO_4	
Mo_2C nanoparticles[19]	198	0.5 M H_2SO_4	*J. Mater. Chem. A,* **2015**, *3,* 8361
Mo_2C nanoparticles[19]	200	1M KOH *ACS Catal.* **2014**, *4,* 2658	*J. Mater. Chem. A,* **2015**, *3,* 8361
Mo_2C nanowires[20]	200	0.5 M H_2SO_4	*Electrochim. Acta,* **2014**, *134,* 182
Mo_2C nanorod[21]	150	0.5 M H_2SO_4	*Appl. Catal. B: Environ.* **2014**, *154-155,* 232.
Ni impregnated Mo_2C nanorod[21]	130	1M KOH	*Appl. Catal. B: Environ.* **2014**, *154-155,* 232.
Mo_2C–NCNTs[22]	147	0.5 M H_2SO_4	*J. Mater. Chem. A,* **2015**, *3,* 5783
Mo_2C–NCNTs[22]	257	1M KOH	*J. Mater. Chem. A,* **2015**, *3,* 5783
Mo_2C–RGO[23]	130	0.5 M H_2SO_4	*Chem. Commun.,* **2014**, *50,* 13135.
N, P-doped Mo_2C@C[24]	47	1M KOH	*ACS Nano* **2016**, *10,* 8851.
Mo_2C[25]	210	1 M H_2SO_4	*Angew. Chem. Int. Ed.* **2012**, *51,* 12703.
Mo_2C[25]	190	1M KOH	*Angew. Chem. Int. Ed.* **2012**, *51,* 12703.
Mo_2C/CN[26]	140	0.5 M H_2SO_4	*ChemCatChem* **2018**, *10,* 625

Table S7 Summary of the electrocatalytic HER performance of different high-performance catalysts.

catalyst	overpotential η at j = 10 mA cm^{-2} (mV)	electrolyte	reference
β-Mo_2C@NPCC	80	0.5 M H_2SO_4	This work
β-Mo_2C@NPCC	132	1 M KOH	This work
Nanocrystalline Ni_5P_4[27]	50	1 M NaOH	*Energy Environ. Sci.* **2015**, *8*, 1027
TiO_2NDs/CoNSNTs-CFs[28]	108	1 M KOH	*Angew. Chem. Int. Ed.* **2017**, 56, 2960
$NiCo_2O_4$ hollow microcuboids[29]	110	1 M NaOH	*Angew. Chem. Int. Ed.* **2016**, *55,* 6290
1T-$MoSe_2$[30]	152	0.5 M H_2SO_4	*Adv. Mater.* **2017**, *29,* 1700311
FeP/C[31]	71	0.5 M H_2SO_4	*J. Am. Chem. Soc.,* **2017**, *139,* 6669
$Ni_{0.89}Co_{0.11}Se_2$ MNSN/NF[32]	52	0.5 M H_2SO_4	*Adv. Mater.* **2017**, *29,* 1606521
$Ni_{0.89}Co_{0.11}Se_2$ MNSN/NF[32]	85	1 M KOH	*Adv. Mater.* **2017**, *29,* 1606521
TiN@Ni_3N[33]	120	1 M KOH	*J. Mater. Chem. A* **2016**, *4,* 5713
c-$CoSe_2$[34]	200	1 M KOH	*Adv. Mater.* **2016**, *28,* 7527
Ni_5P_4 film[35]	150	1 M KOH	*Angew. Chem. Int. Ed.* **2015**, *54,* 12361
NiO/Ni-CNT[36]	80	1 M KOH	*Nat. Commun.* **2014**, *5*, 4695
Ni-Mo nanopowder[37]	～63	2 M KOH	*ACS Catal.* **2013**, *3,* 166
MoP[38]	130	1 M KOH	*Energy Environ. Sci.* **2014**, *7,* 2624
MoP Net work[39]	125	0.5 M H_2SO_4	*Adv. Mater.* **2014**, *26*, 5702
Co-NRCNTs[40]	140	0.5 M H_2SO_4	*Angew. Chem. Int. Ed.* **2014**, 53, 4372
IrCo@NC-500[41]	24	0.5 M H_2SO_4	*Adv. Mater.* **2018**, *30,* 1705324
IrCo@NC-500[41]	45	1 M KOH	*Adv. Mater.* **2018**, *30,* 1705324
CoP NCs[42]	62.5	1 M KOH	*Adv. Mater.* **2018**, *30*, 1705796
Co−C−N[43]	138	0.5 M H_2SO_4	*J. Am. Chem. Soc.*, **2015**, *137*, 15070

References

1. B. Ravel and M. Newville, *J. Synchrotron Radiat.*, 2005, **12**, 537-541.
2. G. Kresse and J. Furthmüller, *Phys. Rev. B*, 1996, **54**, 11169-11186.
3. J. P. Perdew, K. Burke and M. Ernzerhof, *Phys. Rev. Lett.*, 1996, **77**, 3865-3868.
4. P. E. Blöchl, *Phys. Rev. B*, 1994, **50**, 17953-17979.
5. E. Parthe and V. Sadogopan, *Acta Cryst.*, 1963, **16**, 202-205.
6. P. J. Linstrom and W. Mallard, NIST Chemistry WebBook, NIST Standard Reference Database Number 69, ed., National Institute of Standards and Technology, Gaithersburg MD, 2001, 20899.
7. C. J. Cramer, *Essentials of computational chemistry: theories and models*, John Wiley & Sons, 2004.
8. Y. Liu, G. Yu, G. D. Li, Y. Sun, T. Asefa, W. Chen and X. Zou, *Angew. Chem. Int. Ed.*, 2015, **54**, 10752-10757.
9. H. B. Wu, B. Y. Xia, L. Yu, X. Y. Yu and X. W. Lou, *Nat. Commun.*, 2015, **6**, 6512.
10. Y. Zhao, K. Kamiya, K. Hashimoto and S. Nakanishi, *J. Am. Chem. Soc.*, 2015, **137**, 110-113.
11. H. Zhang, Z. Ma, G. Liu, L. Shi, J. Tang, H. Pang, K. Wu, T. Takei, J. Zhang, Y. Yamauchi and J. Ye, *NPG Asia Mater.*, 2016, **8**, e293.
12. F. X. Ma, H. B. Wu, B. Y. Xia, C. Y. Xu and X. W. Lou, *Angew. Chem. Int. Ed.*, 2015, **54**, 15395-15399.
13. C. Wan, Y. N. Regmi and B. M. Leonard, *Angew. Chem. Int. Ed.*, 2014, **53**, 6407-6410.
14. D. H. Youn, S. Han, J. Y. Kim, J. Y. Kim, H. Park, S. H. Choi and J. S. Lee, *ACS Nano*, 2014, **8**, 5164-5173.

15. L. Liao, S. Wang, J. Xiao, X. Bian, Y. Zhang, M. D. Scanlon, X. Hu, Y. Tang, B. Liu and H. H. Girault, *Energy Environ. Sci.*, 2014, **7**, 387-392.
16. W. F. Chen, C. H. Wang, K. Sasaki, N. Marinkovic, W. Xu, J. T. Muckerman, Y. Zhu and R. R. Adzic, *Energy Environ. Sci.*, 2013, **6**, 943.
17. J. Zhang, X. Meng, J. Zhao and Z. Zhu, *ChemCatChem*, 2014, **6**, 2059-2064.
18. W. Cui, N. Cheng, Q. Liu, C. Ge, A. M. Asiri and X. Sun, *ACS Catal.*, 2014, **4**, 2658-2661.
19. L. Ma, L. R. L. Ting, V. Molinari, C. Giordano and B. S. Yeo, *J. Mater. Chem. A*, 2015, **3**, 8361-8368.
20. C. Ge, P. Jiang, W. Cui, Z. Pu, Z. Xing, A. M. Asiri, A. Y. Obaid, X. Sun and J. Tian, *Electrochim. Acta*, 2014, **134**, 182-186.
21. P. Xiao, Y. Yan, X. Ge, Z. Liu, J.-Y. Wang and X. Wang, *Appl. Catal., B*, 2014, **154-155**, 232-237.
22. K. Zhang, Y. Zhao, D. Fu and Y. Chen, *J. Mater. Chem. A*, 2015, **3**, 5783-5788.
23. L. F. Pan, Y. H. Li, S. Yang, P. F. Liu, M. Q. Yu and H. G. Yang, *Chem. Commun.*, 2014, **50**, 13135-13137.
24. Y. Y. Chen, Y. Zhang, W. J. Jiang, X. Zhang, Z. Dai, L. J. Wan and J. S. Hu, *ACS Nano*, 2016, **10**, 8851-8860.
25. H. Vrubel and X. Hu, *Angew. Chem. Int. Ed.*, 2012, **51**, 12703-12706.
26. M. Fan, Y. Zheng, A. Li, Y. Ma, Q. Huo, Z.-A. Qiao and S. Dai, *ChemCatChem*, 2018, **10**, 625-631.
27. A. B. Laursen, K. R. Patraju, M. J. Whitaker, M. Retuerto, T. Sarkar, N. Yao, K. V. Ramanujachary, M. Greenblatt and G. C. Dismukes, *Energy Environ. Sci.*, 2015, **8**, 1027-1034.
28. J. X. Feng, H. Xu, Y. T. Dong, X. F. Lu, Y. X. Tong and G. R. Li, *Angew. Chem. Int. Ed.*, 2017, **56**, 2960-2964.
29. X. Gao, H. Zhang, Q. Li, X. Yu, Z. Hong, X. Zhang, C. Liang and Z. Lin, *Angew. Chem. Int. Ed.*, 2016, **55**, 6290-6294.
30. Y. Yin, Y. Zhang, T. Gao, T. Yao, X. Zhang, J. Han, X. Wang, Z. Zhang, P. Xu, P. Zhang, X. Cao, B. Song and S. Jin, *Adv. Mater.*, 2017, **29**, 1700311.
31. D. Y. Chung, S. W. Jun, G. Yoon, H. Kim, J. M. Yoo, K. S. Lee, T. Kim, H. Shin, A. K. Sinha, S. G. Kwon, K. Kang, T. Hyeon and Y. E. Sung, *J. Am. Chem. Soc.*, 2017, **139**, 6669-6674.
32. B. Liu, Y. F. Zhao, H. Q. Peng, Z. Y. Zhang, C. K. Sit, M. F. Yuen, T. R. Zhang, C. S. Lee and W. J. Zhang, *Adv. Mater.*, 2017, **29**, 1606521.
33. Q. Zhang, Y. Wang, Y. Wang, A. M. Al-Enizi, A. A. Elzatahry and G. Zheng, *J. Mater. Chem. A*, 2016, **4**, 5713-5718.
34. P. Chen, K. Xu, S. Tao, T. Zhou, Y. Tong, H. Ding, L. Zhang, W. Chu, C. Wu and Y. Xie, *Adv. Mater.*, 2016, **28**, 7527-7532.
35. M. Ledendecker, S. Krick Calderon, C. Papp, H. P. Steinruck, M. Antonietti and M. Shalom, *Angew. Chem. Int. Ed.*, 2015, **54**, 12361-12365.
36. M. Gong, W. Zhou, M.-C. Tsai, J. Zhou, M. Guan, M.-C. Lin, B. Zhang, Y. Hu, D.-Y. Wang, J. Yang, S. J. Pennycook, B.-J. Hwang and H. Dai, *Nat. Commun.*, 2014, **5**, 4695.
37. J. R. McKone, B. F. Sadtler, C. A. Werlang, N. S. Lewis and H. B. Gray, *ACS Catal.*, 2013, **3**, 166-169.
38. P. Xiao, M. A. Sk, L. Thia, X. Ge, R. J. Lim, J.-Y. Wang, K. H. Lim and X. Wang, *Energy Environ. Sci.*, 2014, **7**, 2624-2629.
39. Z. Xing, Q. Liu, A. M. Asiri and X. Sun, *Adv. Mater.*, 2014, **26**, 5702-5707.
40. X. Zou, X. Huang, A. Goswami, R. Silva, B. R. Sathe, E. Mikmekova and T. Asefa, *Angew. Chem. Int. Ed.*, 2014, **53**, 4372-4376.
41. P. Jiang, J. Chen, C. Wang, K. Yang, S. Gong, S. Liu, Z. Lin, M. Li, G. Xia, Y. Yang, J. Su and Q. Chen, *Adv. Mater.*, 2018, **30**, 1705324.
42. H. Li, Q. Li, P. Wen, T. B. Williams, S. Adhikari, C. Dun, C. Lu, D. Itanze, L. Jiang, D. L. Carroll, G. L. Donati, P. M. Lundin, Y. Qiu and S. M. Geyer, *Adv. Mater.*, 2018, **30**, 1705796.
43. Z. L. Wang, X. F. Hao, Z. Jiang, X. P. Sun, D. Xu, J. Wang, H. X. Zhong, F. L. Meng and X. B. Zhang, *J. Am. Chem. Soc.*, 2015, **137**, 15070-15073.